



# Analytical and computational solutions for three-dimensional flow-field and relative pathlines for the rotating flow in a Tesla disc turbine



Sayantan Sengupta, Abhijit Guha\*

Mechanical Engineering Department, Indian Institute of Technology, Kharagpur, Kharagpur 721302, India

## ARTICLE INFO

### Article history:

Received 22 December 2012  
Received in revised form 18 June 2013  
Accepted 8 September 2013  
Available online 19 September 2013

### Keywords:

Tesla turbine  
Absolute pathline  
Relative pathline  
3-D CFD simulation  
Flow reversal

## ABSTRACT

The three-dimensional flow field and the flow pathlines within a Tesla disc turbine have been investigated analytically and computationally. The description of the flow field includes the three-dimensional variation of the radial velocity, tangential velocity and pressure of the fluid in the flow passages within the rotating discs. A detailed comparison between the results obtained from the analytical theory and computational fluid dynamic (CFD) solutions of Navier–Stokes equations is presented in order to establish the reliability of the simplified mathematical model. The present work reveals the dependence of the shape, size and orientation of the pathlines on various operating parameters (such as tangential speed ratio, radial pressure drop, inlet nozzle angle, and position of the exit) and local balance of various forces (viz. inertial, viscous, centrifugal and Coriolis). The relative merits of two possible ways of representing the pathlines in the absolute and relative frame of reference are discussed that provide physical understanding of subtle flow features.

© 2013 Elsevier Ltd. All rights reserved.

## 1. Introduction

The study of detecting and analysing fluid path is important in various fields of fluid dynamics, such as in atmospheric science and oceanography. The direction of wind flow and ocean current is seriously affected by the rotation of the earth. When fluid travels over a relative rotational frame of reference it acquires extra components of inertia force, viz. centrifugal and Coriolis force which cannot be realised in the inertial frame of reference. The role of centrifugal force is to push the fluid in a radially outward direction, whereas the role of Coriolis force is to bend the fluid in a particular direction depending on the direction of fluid velocity and sense of rotation of the reference frame. American meteorologist Ferrel [1] had shown how fluid flow both in the Northern and Southern Hemisphere is deflected due to the effect of Coriolis force. Such deflections and many other flow physics can be captured by the flow visualisation technique. In fluid dynamics, the pattern of flow can be visualised in various ways such as streamline, pathline, streakline, timeline etc. Presently, the visualisation of fluid flow in turbomachinery (see [2–5], etc.) is an active area of research. In this paper, fluid flow pattern within a special type of turbomachinery, viz. Tesla turbine [6], invented by the famous scientist Nikola Tesla has been investigated. With this aim, the three-dimensional fluid flow field within the Tesla turbine has been computed here both numerically by the application of computational

fluid dynamics as well as analytically by the application of a mathematical theory developed in [7]. In this context, a brief description about Tesla turbine is provided below for the convenience of understanding of the readers.

Tesla turbine is a bladeless turbo-machinery in which the rotor is constructed by a series of co-axial, parallel flat discs. The discs are attached to a central shaft maintaining a small gap among one another. The combination of discs and shaft is placed inside a cylindrical casing with a small radial and axial clearance. The working fluid is injected nearly tangentially to the rotor by means of one or more inlet nozzle. There are exit ports near the shaft at the centre of each disc.

Tesla turbine can generate power for variety of working media like Newtonian fluids, non-Newtonian fluids, mixed fluids, particle laden two-phase flows [8] (many aspects of two-phase flow may be found in Refs. [9,10]). This turbine has self-cleaning nature due the centrifugal force field. This makes it possible to operate the turbine in case of nonconventional fuels like biomass which produce solid particles.

Currently the field of micro-turbine is an active research area; the bladeless Tesla turbine because of its simplicity and robustness of structure, low cost and comparatively better operation at high rpm may become a very suitable candidate for this application. For this to happen the efficiency of the Tesla turbine, however has to be improved. Researchers are attempting to achieve this by modification of the configuration of the conventional Tesla turbines [8].

The fluid flow in contact with a rotating disc has been the subject-matter of many previous studies, both theoretical and experimental. The problem has attracted some of the greatest minds in

\* Corresponding author.

E-mail address: [a.guha@mech.iitkgp.ernet.in](mailto:a.guha@mech.iitkgp.ernet.in) (A. Guha).



- (3) To provide a clear physical picture how the shape (including complex non-spiral form), length and orientation of pathlines inside the narrow disc gap of a Tesla disc turbine depend on various operating parameters.
- (4) To reveal the dependency of the shape of the pathlines on the local balance of various components of forces.
- (5) To identify the benefit of relative description over absolute description of pathline in light of determining subtle fluid dynamics occurring in a Tesla disc turbine.

## 2. Mathematical formulation

In this section, a mathematical model is outlined, from which the velocity and pressure fields can be calculated. Once the velocity field is known the pathlines can be calculated numerically. The dependency of the shape, length and orientation of pathlines on various operating parameters, and the physical interpretation of the pathlines will be clearer in the subsequent analysis and discussion.

The continuity equation, the momentum equations and boundary conditions are written in terms of relative velocities. For this purpose the following relations between the absolute and relative velocities are used:  $U_r = V_r$ ;  $U_z = V_z$ ;  $U_\theta = (V_\theta + \Omega r)$ . Based on a few assumptions and an order of magnitude analysis (described fully in [7], the conservation equations can be consistently simplified to take the following form.

$$\text{Continuity equation } \frac{\partial V_r}{\partial r} + \frac{V_r}{r} = 0 \quad (1)$$

$$\theta - \text{Momentum equation } V_r \frac{\partial V_\theta}{\partial r} + \frac{V_r V_\theta}{r} + 2\Omega V_r = v \frac{\partial^2 V_\theta}{\partial z^2} \quad (2)$$

$$\begin{aligned} r - \text{Momentum equation } V_r \frac{\partial V_r}{\partial r} - \Omega^2 r - 2\Omega V_\theta - \frac{V_\theta^2}{r} \\ = -\frac{1}{\rho} \frac{dp}{dr} + v \frac{\partial^2 V_r}{\partial z^2} \end{aligned} \quad (3)$$

$$z - \text{Momentum equation } \frac{\partial P}{\partial z} = 0 \quad (4)$$

$$\text{Boundary conditions at } r = r_2 \quad \bar{V}_r = \bar{V}_{r2} \quad \bar{V}_\theta = \bar{V}_{\theta2} \quad (5)$$

$$\text{at } z = 0, b \quad V_r = 0 \quad V_\theta = 0 \quad (6)$$

$$\text{at } z = b/2 \quad \frac{\partial V_r}{\partial z} = \frac{\partial V_\theta}{\partial z} = 0 \quad (7)$$

Eqs. (1)–(3) represent the generalised governing equations developed by the present authors to describe the rotating flow within a Tesla disc turbine, but further simplifications may be possible for specific geometries. Within the boundary layer developed on the flat solid discs, the relative tangential and radial velocities at any radius between  $r_1$  and  $r_2$  can be modelled as

$$V_\theta(r, z) = \bar{V}_{\theta2} \zeta(R) G(z) \quad (8)$$

$$V_r(r, z) = \bar{V}_{r2} \xi(R) H(z) \quad (9)$$

where

$$R = \frac{r}{r_2}, \quad \zeta(R) = \frac{\bar{V}_\theta(r)}{\bar{V}_{\theta2}}, \quad \xi(R) = \frac{\bar{V}_r(r)}{\bar{V}_{r2}}, \quad G(z) = \frac{V_\theta(r, z)}{\bar{V}_{\theta2} \zeta(R)} \quad \text{and} \quad H(z) = \frac{V_r(r, z)}{\bar{V}_{r2} \xi(R)}.$$

$G$  and  $H$  are respectively the  $z$ -variation of tangential and radial velocities within the boundary layers. Here we assume that the velocity profile is parabolic in nature. The reasons behind the above assumptions are clearly described in [7].

Accordingly,  $G$  and  $H$  are as expressed as,

$$G = 6 \frac{z}{b} \left(1 - \frac{z}{b}\right), \quad (10)$$

$$H = 6 \frac{z}{b} \left(1 - \frac{z}{b}\right), \quad (11)$$

$\xi(R)$  is calculated by the integration of continuity equation:

$$\xi(R) = \frac{\bar{V}_r(r)}{\bar{V}_{r2}} = \frac{r_2}{r} \quad (12)$$

Lemma et al. [24] measured this variation in  $\bar{V}_{r2}$  and found that, for a particular pressure drop between the rotor inlet and the exit,  $\bar{V}_{r2}$  is maximum when the rotor is stationary and its magnitude decreases linearly (up to 0.7 bar pressure drop) with  $\Omega$  as given by:

$$-\bar{V}_{r2} = A - B\Omega. \quad (13)$$

In Eq. (13),  $A$  is the maximum inlet radial velocity for stationary rotor, and  $B$  is the slope to be determined by the ratio of the maximum inlet radial velocity for stationary rotor ( $A$ ) to the rotational speed of rotor for which no flow condition is arrived ( $\Omega_0$ ).

We introduce the following three non-dimensional variables for further theoretical development:

$$p' = \frac{p - p_2}{\rho \Omega^2 r_2^2}, \quad \varphi_2 = \frac{\bar{V}_{r2}}{\Omega r_2}, \quad \gamma = \frac{\bar{U}_{\theta2}}{\Omega r_2} \quad (14)$$

The  $\theta$ -momentum Eq. (2) is integrated partially with respect to  $z$  over the domain  $(0, b/2)$ , giving:

$$\frac{d\zeta}{dR} = -\left\{ \frac{1}{R} + 10 \left( \frac{v}{\Omega b^2} \right) \frac{R}{\varphi_2} \right\} \zeta - \frac{10}{6(\gamma - 1)} \quad (15)$$

To avoid singularity of the solution of  $\zeta$  at  $\gamma = 1$  a new variable  $\zeta_m$  is introduced, where  $\zeta_m = \zeta(\gamma - 1)$

$$\frac{d\zeta_m}{dR} = -\left\{ \frac{1}{R} + 10 \left( \frac{v}{\Omega b^2} \right) \frac{R}{\varphi_2} \right\} \zeta_m - \frac{10}{6} \quad (16)$$

The  $r$ -momentum Eq. (3) is integrated partially with respect to  $z$  over the domain  $(0, b/2)$ , resulting in:

$$\frac{dp'}{dR} = R + 2\zeta_m + \frac{6}{5} \frac{\zeta_m^2}{R} + \frac{6}{5} \frac{\varphi_2^2}{R^3} - 12 \left( \frac{v}{\Omega b^2} \right) \frac{\varphi_2}{R} \quad (17)$$

Eq. (13) is substituted in the Eqs. (16) and (17) and these two ODEs are solved for the initial conditions given below

$$\text{At } R = 1 : \zeta_m = \gamma - 1 \quad (18)$$

$$\text{At } R = 1 : p' = 0 \quad (19)$$

The solutions of the above two Eqs. (16) and (17) will give  $\zeta_m$  and  $p'$ . Eqs. (16) and (17) can be integrated simultaneously by numerical means. A simple iterative scheme may be adopted as follows. Assume a value of  $\gamma$  for which the steady state solution is sought. Start with a trial value of  $\Omega$ . Eqs. (16) and (17) are then numerically integrated from the rotor inlet to the exit. The computed value of the pressure drop will not, in general, agree with the imposed value of  $\Delta p_{ic}$ . The value of  $\Omega$  is then systematically varied until the iteration converges to the given value of  $\Delta p_{ic}$ . The same procedure is repeated for various values of  $\gamma$ . It can be seen for various steady state of the rotor that  $\gamma$  decreases monotonically with increase of  $\Omega$ .

The full derivation of the mathematical model is given by Sengupta and Guha [7] which also provide experimental verification of the mathematical theory.

## 3. Computation of path line in the relative frame

Absolute and relative pathlines are two possible ways of representing the fluid motion inside the narrow disc-gap of a Tesla disc turbine. The first one, i.e. absolute pathline can be observed by a stationary observer standing outside the rotational frame of reference. On the other hand, relative pathlines can only be observed if the observer is moving at the same angular velocity as that of the rotor. Relative pathlines can be calculated from the present analytical theory since it gives the three-dimensional variation of  $V_\theta$  and  $V_r$  within a Tesla disc turbine. A code written by finite difference

method is utilised to calculate a single path line from inlet to exit for any particular rotational speed of the rotor. For computation of the relative pathlines a plane is chosen where the tangential and radial velocities at any radial location are equal to the  $z$ -averaged tangential and radial velocities (or in other words,  $V_\theta = \bar{V}_\theta$  and  $V_r = \bar{V}_r$ ). The time taken by the working fluid to reach from inlet to exit is divided into small steps. At each instant of time,  $\bar{V}_\theta$  and  $\bar{V}_r$  can be calculated from the present theory since the  $(r, \theta)$  co-ordinate of the fluid particle is known from the numerical integration at the previous time step. As  $\bar{V}_r$  is known, the radial distance travelled by the fluid during a time step can be calculated and the change in the value of  $\theta$  can be computed numerically from  $\tan^{-1}(\bar{V}_r/\bar{V}_\theta)$ . Successive application of this procedure enables one to trace the pathline (in the relative frame) completely from the inlet to the outlet.

**4. Effect of various parameters on the relative pathline**

The shape, size and orientation of the pathlines are dependent on the velocity field which, in turn, depends on the geometry and various operating parameters. The following sections explore the nature of such dependence. Unless otherwise stated at the respective places, the following parameters are adopted from the experimental study of Lemma et al. [24] for all example analytical results given here:  $r_2 = 25$  mm,  $r_1 = 13.2$  mm,  $b = 0.46$  mm,  $\Delta p_{ic} = 0.113$  bar. Air is considered as the working fluid.

**4.1. Effect of tangential speed ratio ( $\gamma$ )**

The definition of tangential speed ratio  $\gamma$  has been introduced in the Eq. (14) of Section 2. The working fluid enters nearly tangentially through the narrow disc-gap of the rotor. For particular values of  $\gamma$  and  $\Delta p_{ic}$ , the steady state corresponds to particular values of  $\Omega$  (rotational speed of the discs) and  $\bar{U}_{\theta 2}$  (the average absolute tangential velocity of the fluid at the rotor inlet). Generally, the peripheral velocity of the rotor ( $\Omega r_2$ ) is not same with the value of  $\bar{U}_{\theta 2}$  and  $\gamma$  can be greater, less or equal to one. Figs. 2a and 2b, and Fig. 3 show the variation of the relative pathlines with  $\gamma$ , while the geometry of the turbine and  $\Delta p_{ic}$  are kept constant. Fig. 2a shows that, for  $\gamma \geq 1$ , the fluid moves spirally in the direction of

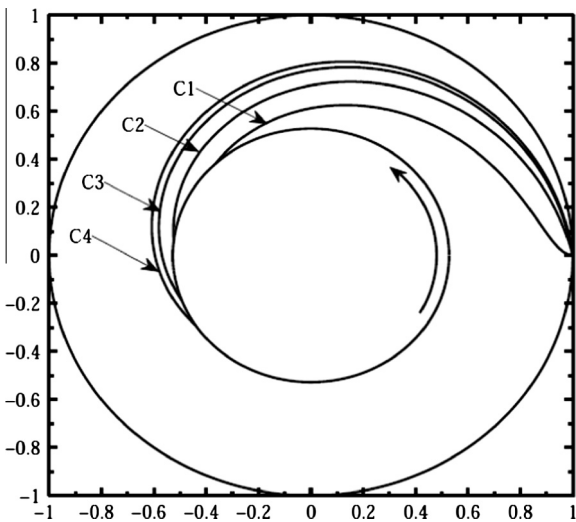


**Fig. 2a.** Effect of various tangential speed ratio (considering cases when  $\gamma \geq 1$ ) on relative pathline computed from inlet ( $R = 1$ ) to exit ( $R = 0.528$ ): prediction of the present theory. C1: Relative pathline for  $\gamma = 1.5$ , C2: Relative pathline for  $\gamma = 1$ , C3: Relative pathline for  $\gamma = 3$ , C4: Relative pathline for  $\gamma = 10$ . [Arrow represents direction of rotation of the disc. For all calculations  $\Delta p_{ic} = 0.113$  bar.]

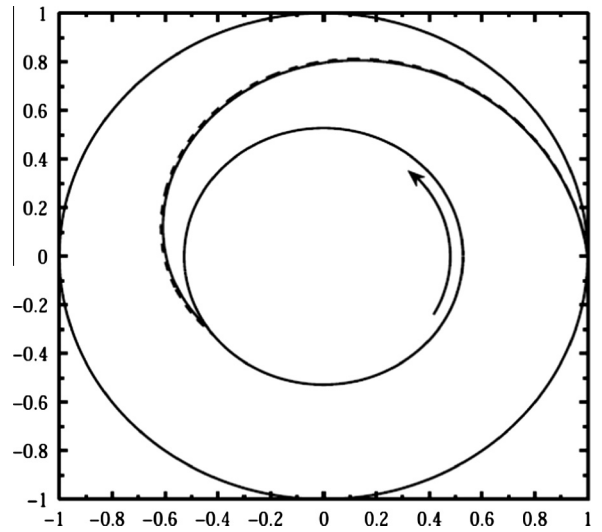


**Fig. 2b.** Relative pathline from inlet ( $R = 1$ ) to exit ( $R = 0.528$ ) computed at  $\gamma = 10$  (represented by solid line) and  $\gamma = 50$  (represented by dotted line) when  $\Delta p_{ic} = 0.113$  bar: arrow represents direction of rotation of the disc.

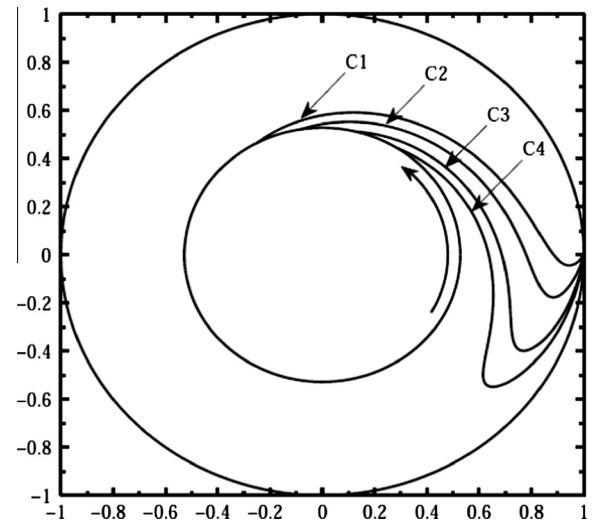


**Fig. 3.** Effect of various tangential speed ratio (considering cases when  $\gamma < 1$ ) on relative pathline computed from inlet ( $R = 1$ ) to exit ( $R = 0.528$ ): prediction of the present theory. C1: Relative pathline for  $\gamma = 0.9$ , C2: Relative pathline for  $\gamma = 0.8$ , C3: Relative pathline for  $\gamma = 0.7$ , C4: Relative pathline for  $\gamma = 0.64$ . [Arrow represents direction of rotation of the disc. All curves show flow reversal. For all calculations  $\Delta p_{ic} = 0.113$  bar.]

the disc rotation (anticlockwise in the present example). As the value of  $\gamma$  increases, the length of the relative pathline increases, though the increase is modest even when  $\gamma$  is changed by a large factor. A general expectation could be that such trend is maintained until the value of  $\Omega$  becomes zero. [In this context, for the clarity of understanding, it may be remembered that the steady state value of  $\Omega$  decreases monotonically with the increase of  $\gamma$  (as discussed Section 2)]. However, Fig. 2b shows that the length, shape and orientation of the pathlines become insensitive to changes in  $\gamma$  when  $\gamma$  is adequately large. There are two main reasons for which the length of the pathline (calculated in the relative frame of reference) increases with the increase of  $\gamma$ . First of all,  $\bar{V}_{\theta 2}$  increases with the increase of  $\gamma$ .

Secondly,  $\bar{V}_{r 2}$  decreases with the increase of  $\gamma$  (see, Eq. (13)).

Fig. 3 shows that for each  $\gamma < 1$ , a fluid particle first (i.e. in the inlet region) moves opposite to the direction of disc rotation, then

(near outlet region) it moves in the same sense as the disc rotation. This interesting shape of the pathline in the relative frame occurs due to the occurrence of flow reversal. In the region between the rotor inlet (at point 2) and the point of flow reversal, the rotor disc would absorb power, instead of delivering. However, the disc would develop positive power in the region between the point of flow reversal and the rotor outlet ( $R_1$ ). If the positive power is more than the negative power, then the rotor disc would produce a net power output and the Tesla turbine would remain functional. Hence, it is very much possible that a Tesla turbine remains working even at  $\gamma < 1$ . The flow transition in the relative frame is possible only due to the effect of Coriolis acceleration. It can be shown that starting from an initial negative value,  $\bar{V}_\theta$  would always remain negative due the individual effect of either viscous force or the conservation of angular momentum. The subtle role of Coriolis force for flow reversal had been discussed extensively in [20]. Another important feature revealed from Fig. 3 is that the reversal point shifts towards the exit radius ( $R_1$ ) as the value of  $\gamma$  decreases. The flow physics described in this paragraph indicates that a no-torque condition would appear at a particular value of  $\gamma$ . This limiting value of  $\gamma$  can be calculated from the analytical formula

$$[\gamma]_{no\ torque} = 1 - \frac{10}{6} \left[ \frac{C_1 \frac{(1-R_1^2)}{2} + \{1 - \exp[\frac{C_1}{2}(1-R_1^2)]\}}{C_1 \{1 - \exp[\frac{C_1}{2}(1-R_1^2)]\}} \right] \quad (20)$$

(where,  $C_1 = \frac{10v}{\phi_2 \Omega b^2}$ ).

#### 4.2. Effect of the pressure difference between inlet and exit of the rotor ( $\Delta p_{ic}$ )

Figs. 4a and 4b show how the characteristics of relative pathlines depend on the pressure drop ( $\Delta p_{ic}$ ) between the inlet and the exit of the rotor, for particular values of  $\gamma$  and  $\alpha_n$ , and for a specific geometry of Tesla turbine. Figs. 4a and 4b reveal the fact that the effect of increasing  $\Delta p_{ic}$  up to a certain extent leads to the increase of the length of relative pathlines. However, any further increase of  $\Delta p_{ic}$  shortens the length of the relative pathline. The physical reasons for this behaviour can be explained as follows.

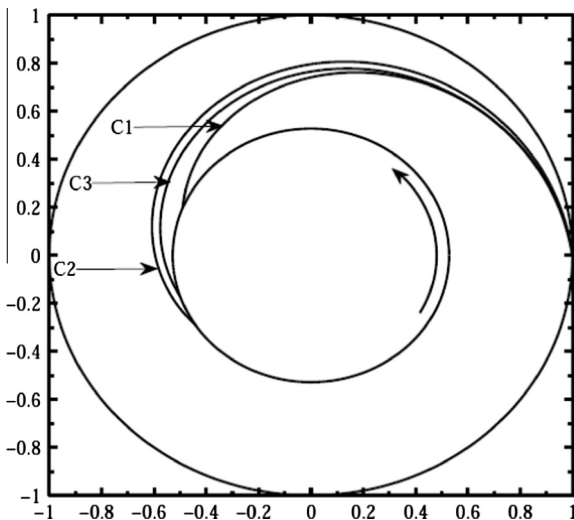


Fig. 4a. Effect of various  $\Delta p_{ic}$  on relative pathline computed from inlet ( $R = 1$ ) to exit ( $R = 0.528$ ): prediction of the present theory. C1: Relative pathline for  $\Delta p_{ic} = 0.03$  bar, C2: Relative pathline for  $\Delta p_{ic} = 0.113$  bar, C3: Relative pathline for  $\Delta p_{ic} = 0.313$  bar. [Arrow represents direction of rotation of the disc. For all calculations  $\gamma = 10$ .]

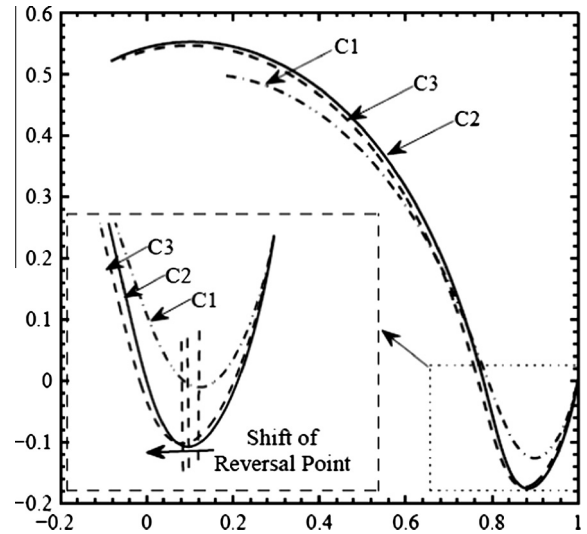


Fig. 4b. Effect of various  $\Delta p_{ic}$  on relative pathline computed from inlet ( $R = 1$ ) to exit ( $R = 0.528$ ): prediction of the present theory. C1: Relative pathline for  $\Delta p_{ic} = 0.03$  bar, C2: Relative pathline for  $\Delta p_{ic} = 0.113$  bar, C3: Relative pathline for  $\Delta p_{ic} = 0.313$  bar. [Direction of rotation of the disc is considered to be anticlockwise. For all calculations  $\gamma = 0.8$ .]

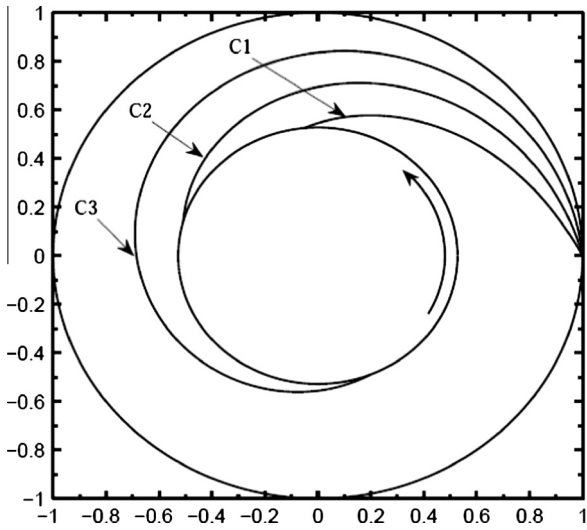
Suppose, atmospheric pressure is maintained at the exit plane and  $\Delta p_{ic}$  is increased by increasing the inlet pressure of the rotor. As a consequence, the absolute velocity at inlet will also increase. Generally, the length of the relative pathlines (for this flow domain) increases due to the increase of relative tangential velocity, whereas it decreases due to the increase of the magnitude of radial velocity. If the effect of increase of radial velocity overtakes the effect of increase of relative tangential velocity the length of the pathlines decreases.

Fig. 4a shows pathlines calculated for a specific value of  $\gamma$  which is greater than one and Fig. 4b shows pathlines calculated for a specific value of  $\gamma$  which is less than one (when flow reversal occurs). It can be seen that the trend of change in length of the pathlines (with the change in  $\Delta p_{ic}$ ) remains the same for  $\gamma$  greater or less than one. Fig. 4b exhibits an additional feature that the point of reversal shifts towards the exit with the increase of pressure drop. An interesting point to note here is that, as the radial pressure drop increases, the point of reversal shifts monotonically towards the centre whereas the length of the relative pathlines initially increases but subsequently decreases with further increase in pressure drop (for the reasons explained previously).

#### 4.3. Effect of nozzle angle ( $\alpha_n$ ) and exit radius

The working fluid is injected in a nearly tangential path by one or more inlet nozzle through the periphery of the rotor of a Tesla disc turbine. In the present analysis, uniform flow rate throughout the periphery is considered. The average tangential and radial component of velocity of the working fluid before entering into the relative rotational frame of reference are  $\bar{U}_{r2}$  and  $\bar{U}_{\theta 2}$  respectively. Therefore, the working fluid enters at an angle of  $\tan^{-1}(\bar{U}_{r2}/\bar{U}_{\theta 2})$  from the inlet nozzle through the periphery of the rotor. After entering into the disc-gap at an angle  $\alpha_n$  the working fluid approaches in spiral path (if  $\gamma > 1$ ) or complex non-spiral path (if  $\gamma < 1$ ) to the exit. The dependence of the characteristics of relative pathlines on the nozzle angle ( $\alpha_n$ ) and the exit radius (radius ratio) is investigated in this section.

In the analysis presented so far, Eq. (13) is applied for the calculation of  $\bar{V}_{r2}$  because the disc geometry and nozzle arrangement



**Fig. 5a.** Effect of various nozzle angle ( $\alpha_n$ ) on relative pathline computed from inlet ( $R = 1$ ) to exit ( $R = 0.528$ ): prediction of the present theory. C1: Relative pathline calculated at  $\alpha_n = 10^\circ$ , C2: Relative pathline calculated at  $\alpha_n = 5^\circ$ , C3: Relative pathline calculated at  $\alpha_n = 2^\circ$ . [Arrow represents direction of rotation of the disc. For all calculations  $\Delta p_{ic} = 0.113$  bar; and  $\gamma = 1.5$ .]

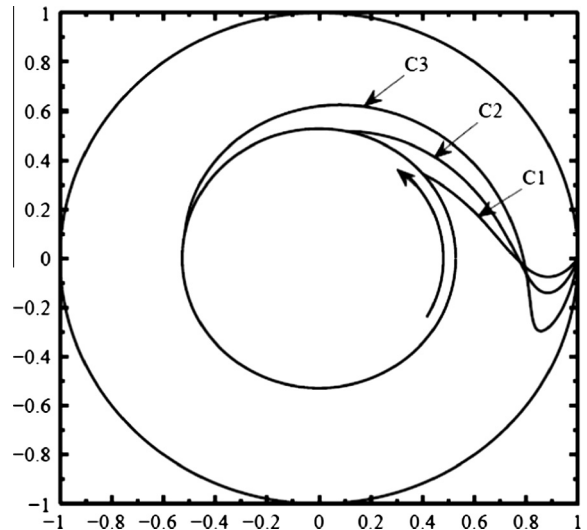


**Fig. 5b.** Effect of various nozzle angle ( $\alpha_n$ ) on relative pathline computed from inlet ( $R = 1$ ) to exit ( $R = 0.528$ ): prediction of the present theory. C1: Relative pathline calculated at  $\alpha_n = 10^\circ$ , C2: Relative pathline calculated at  $\alpha_n = 5^\circ$ , C3: Relative pathline calculated at  $\alpha_n = 2^\circ$ . [Arrow represents direction of rotation of the disc. For all calculations  $\Delta p_{ic} = 0.113$  bar and  $\gamma = 0.8$ .]

are the same as that used in the experimental measurements by Lemma et al. [24]. However, Eq. (13) cannot be used if the nozzle angle or the disc geometry is altered. Then Eqs. (16) and (17) need to be expressed in terms of nozzle angle  $\alpha_n$  as follows:

$$\frac{d\zeta_m}{dR} = - \left[ \frac{1}{R} + 10 \left( \frac{vr_2}{b^2} \right) \frac{R}{\bar{U}_{02} \tan \alpha_n} \right] \zeta_m - \frac{10}{6} \quad (21)$$

$$\frac{dp'}{dR} = R + 2\zeta_m + \frac{6}{5} \frac{\zeta_m^2}{R} + \frac{6}{5} \frac{\gamma^2 \tan^2 \alpha_n}{R^3} - 12 \left( \frac{vr_2}{b^2} \right) \frac{\gamma^2 \tan \alpha_n}{\bar{U}_{02} R} \quad (22)$$

The numerical procedure for solving Eqs. (21) and (22) with boundary conditions (18) and (19) is similar to that described in Section 2; the only difference here is that, for a particular value of  $\alpha_n$ , one needs to iteratively find the particular value of  $\bar{U}_{02}$  that gives the required pressure drop between the inlet and the exit of the rotor.

Figs. 5a and 5b show how the relative pathlines are dependent on the nozzle angle. The sample calculations are done by varying  $\alpha_n$  from  $2^\circ$  to  $10^\circ$  (while rotor geometry,  $\Delta p_{ic}$  and  $\gamma$  are kept fixed). It can be seen from both Figs. 5a and 5b that the length of the pathlines decreases with the increase in inlet angle. The reason for this is that with the increase of nozzle angle the radial velocity increases and tangential velocity decreases.

Fig. 6 shows that the shape, size and orientation of the relative pathline depend significantly on the radius of exit. The extent of the movement of the working fluid between the narrow disc spaces is governed by the position of the exit (in the present study the position is varied only by changing the outlet radius). Fig. 6 shows that for a particular value of  $\Delta p_{ic}$ ,  $\gamma$ ,  $\alpha_n$  and  $r_2$ , the length of relative pathline increases with the decrease of the radius of the exit. With the decrease of radius of the exit, the absolute tangential velocity<sup>1</sup> at rotor-inlet has to be decreased to maintain a constant  $\Delta p_{ic}$ . In order to keep the nozzle angle fixed, the radial velocity at rotor-inlet is also changed correspondingly. A reduced radial speed would tend to increase the residence time of a fluid particle and hence increase the length of the relative pathline. Similarly,

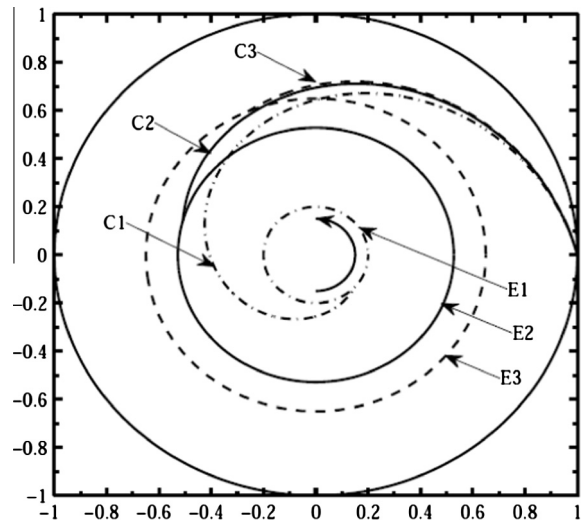


**Fig. 6.** Effect of varying position of exit on relative pathline computed for  $\Delta p_{ic} = 0.113$  bar,  $\gamma = 1.5$  and  $\alpha_n = 5^\circ$ : prediction of the present theory. C1: Relative pathline calculated from inlet ( $R = 1$ ) to exit E1 ( $R = 0.2$ ) [both C1 and E1 are represented by - - - - -], C2: Relative pathline calculated from inlet ( $R = 1$ ) to exit E2 ( $R = 0.528$ ) [both C2 and E2 are represented by —], C3: Relative pathline calculated from inlet ( $R = 1$ ) to exit E3 ( $R = 0.65$ ) [both C3 and E3 are represented by ———]. [Arrow represents direction of rotation of the disc.]

an increased radial extent ( $r_2 - r_1$ ) tends to increase the relative pathline. However, the relative tangential velocity at inlet decreases (alongwith  $\bar{U}_{02}$ ) and this has the opposite effect on the length of the relative pathline. Overall, the length of relative pathline increases with a decrease of the radius of the outlet. It is to be noted that the three pathlines shown in Fig. 6 are different not only in their length but also in their orientation over the common flow domain even though the inlet nozzle angle is maintained at a constant value for all three cases. The local angle depends on the relative magnitudes of the various forces acting on a fluid particle at a particular location, and the relative magnitudes change as the outlet radius is altered.

<sup>1</sup> Remembering that the length of pathline decreases with decrease of  $\bar{U}_{02}$ .

**5. Absolute versus relative pathline**

In this section, a comparative study of the pathlines computed in absolute and relative frames of reference are provided. Fig. 7 shows absolute and relative pathlines of the working fluid from inlet to the exit of the rotor calculated for the same operating conditions and geometric arrangements. The figure shows that the length of the absolute pathline is greater than the length of the relative pathline. Computations for many combinations of geometrical data and input boundary conditions also revealed that the relative pathline reaches the exit plane usually within one complete revolution whereas the absolute pathlines may continue for several revolutions before reaching the exit plane. These observations can be explained from the following three facts:

1. The relations provided in Section 2 show that the absolute and relative radial velocities are same, whereas the relative tangential velocity is always less than the absolute tangential velocity.
2. As the working fluid approaches from inlet to the exit of the rotor, the radial velocity gradually increases due to the gradual decrease of the flow area. On the other hand, the relative tangential velocity may either increase or decrease depending on the value of tangential speed ratio and local balance of the various components of force [20].
3. Under efficient operating conditions, the rotational speed of the rotor is considerably high and therefore the relative tangential component of velocity is usually of the same order of the radial velocity.

It can also be observed from Fig. 7 that the orientation of the relative pathline is different from that of the absolute pathline. It is so because the orientation of the relative pathline is governed by the angle  $\tan^{-1}(V_r/V_\theta)$ , whereas the orientation of the absolute pathline is controlled by the angle  $\tan^{-1}(\bar{U}_r/\bar{U}_\theta)$ . Even though the length of a fluid pathline is shorter in the relative frame, the time taken by a fluid particle to travel from the inlet to the exit is exactly the same in both absolute and relative frames since the radial velocity does not depend on the rotation. Hence, at the same instant of time, both pathlines reach the same radial coordinate but different tangential positions. This tangential movement can be interpreted as the contribution of the Coriolis force in a rotational frame of reference.

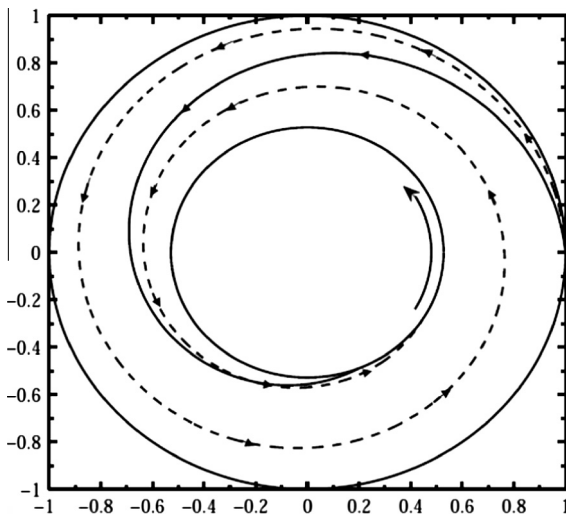


**Fig. 7.** Absolute and relative pathline from inlet ( $R = 1$ ) to exit ( $R = 0.528$ ) computed for  $\Delta p_{ic} = 0.113$  bar,  $\gamma = 1.5$  and  $\alpha_n = 2^\circ$  [— absolute pathline, - - - relative pathline; arrow represents direction of rotation of the disc].

It may seem that the absolute and relative pathlines are merely two different ways of visualising the same flow. Nevertheless, certain subtle flow physics, such as flow reversal and the role of Coriolis force in establishing complex flow features, can only be appreciated when the relative pathlines are analysed.

**6. Computational fluid dynamic simulation of the three-dimensional flow-field**

The fluid flow field within the rotating discs have also been studied by the application of computational fluid dynamics (CFD). A commercially available CFD software, Fluent 6.3.26, is utilised for the present computation. Three dimensional, double precision, pressure based, steady and implicit solver is used. Velocity formulation is in the absolute frame of reference and flow is considered to be laminar. The SIMPLE algorithm, with first order upwind scheme for momentum and ‘Standard’ scheme for discretizing the pressure equation, is utilised. Under-relaxation factors for momentum, pressure, density, and body force are chosen respectively 0.7, 0.3, 1 and 1. The convergence criterion for all residuals is set as  $10^{-11}$ .

The geometry of the model is created by a commercially available software, GAMBIT 2.4.6. Each disc has an outer radius of 25 mm and the inner radius of 13.2 mm, with 0.1 mm inter-disc

**Table 1**  
Grid independence test for  $\Omega = 1000$  rad/s.

Grid distribution	Number of grids in $r$ , $\theta$ and $z$ directions	Total number of grids	Area averaged static pressure at inlet (Pascal)
Coarse	(50 × 190 × 60)	570,000	5234.145
	(100 × 95 × 60)	570,000	5243.292
	(100 × 190 × 30)	570,000	5237.147
Standard	(100 × 190 × 60)	1,140,000	5245.192
Fine	(200 × 190 × 60)	2,280,000	5246.114
	(100 × 380 × 60)	2,280,000	5245.478
	(100 × 190 × 120)	2,280,000	5246.847

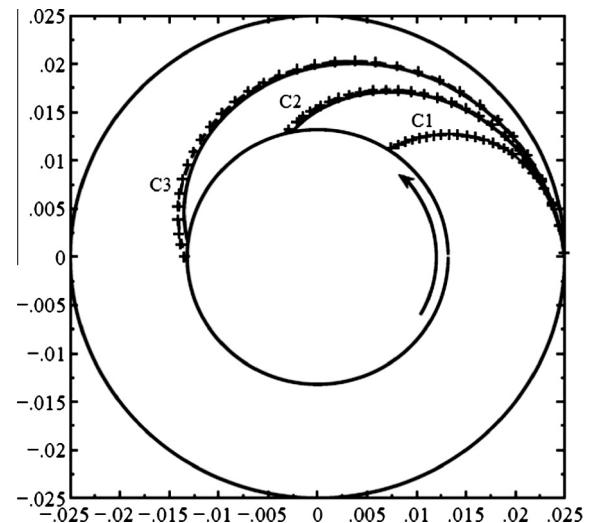


**Fig. 8.** Comparison of prediction of present theory and CFD simulation in determining absolute pathlines from inlet ( $r = 25$  mm) to exit ( $r = 13.2$  mm) for various values of  $\Omega$ . [— prediction of present analytical model, - - - Fluent first order upwind scheme, + + + + Fluent second order upwind scheme. C1: for  $\Omega = 1000$  rad/s,  $\gamma = 4.57$  and  $\alpha_n = 5.75$ ; C2: for  $\Omega = 2500$  rad/s,  $\gamma = 2.03$  and  $\alpha_n = 5.18$ ; C3: for  $\Omega = 4950$  rad/s,  $\gamma = 1.18$  and  $\alpha_n = 4.47$ . Arrow represents direction of rotation of the disc.]

spacing. Numerical simulations are carried out for three different rotational speeds (1000, 2500 and 4950 rad/s) of the disc. At inlet, the maximum tangential velocity  $U_\theta$  (of the parabolic distribution) is specified as 159 m/s and the maximum radial velocity (of the parabolic distribution) is  $-17.25$  m/s. Air with constant density ( $1.225$  kg/m<sup>3</sup>) is chosen as the working fluid.

Incompressible flow has been considered for both analytical and CFD calculations, though the maximum value of the parabolic velocity profile at inlet (the centreline Mach number being 0.46) is slightly above the conventional limit of incompressible flow analysis. There are several reasons for this simplification. With strong

non-uniformity in the  $z$ -direction, it turns out that  $z$ -averaged  $\bar{U}_\theta$  is within the incompressibility limit. Secondly, the numerical solutions show that, for small inter-disc spacing, the value of tangential velocity decreases substantially within a short radial distance (see Fig. 10). Thirdly, the analytical formulation is in terms of relative tangential velocity which is smaller than the absolute tangential velocity.

The outlet boundary condition at the exit radius is modelled as pressure outlet with zero gauge pressure. No slip boundary condition is set on the disc walls. A grid-independence test for  $\Omega = 1000$  rad/s (see Table 1) has been carried out, and based on this study, a total of 1,140,000 mapped, hexahedral computational cells are used for the results presented below (meshing is done in GAMBIT 2.4.6).

Fig. 8 shows the absolute pathlines in the mid-plane of the flow domain for the three rotational speeds of the discs and the particular inlet and outlet conditions as described above. It can be seen from this figure that the pathlines obtained from the numerical simulation are almost coinciding with the pathlines obtained from the mathematical model. Fig. 9 shows that the radial distributions of pressure (gauge pressure) calculated from the mathematical model and the numerical simulation match well. A comparison between the first and second order upwind schemes has been given in Figs. 8 and 9. The comparison shows that, for the adopted grid, the first order upwind scheme is adequate.

Results of CFD simulation within a Tesla disc turbine are represented by Fig. 10 which includes absolute pathlines, contours of pressure, radial velocity and tangential velocity (considering 1000 rad/s rotational speed of the discs and an inter-disc spacing of 100  $\mu$ m). It can be observed from this figure that

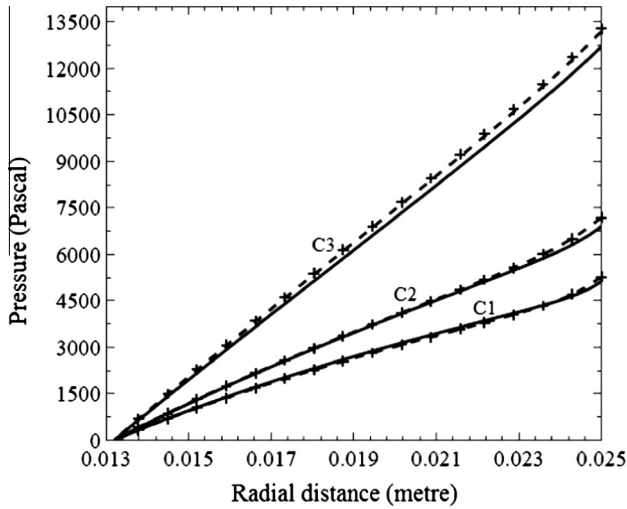


Fig. 9. Comparison of prediction of present theory and CFD simulation in determining radial pressure distribution from inlet ( $r = 25$  mm) to exit ( $r = 13.2$  mm) for various values of  $\Omega$ . [— prediction of present analytical model, ---- Fluent first order upwind scheme, + + + + Fluent second order upwind scheme. C1: for  $\Omega = 1000$  rad/s,  $\gamma = 4.57$  and  $\alpha_n = 5.75$ ; C2: for  $\Omega = 2500$  rad/s,  $\gamma = 2.03$  and  $\alpha_n = 5.18$ ; C3: for  $\Omega = 4950$  rad/s,  $\gamma = 1.18$  and  $\alpha_n = 4.47$ .]

1. Pressure continuously drops in the  $r$ -direction from inlet to outlet (see plane 1 in Fig. 10a).
2. Pressure does not vary in the  $z$ -direction (see plane 2 in Fig. 10a); this verifies Eq. (4).
3. In the  $r$ -direction, the tangential velocity decreases substantially near the inlet (see plane 3 in Fig. 10a).

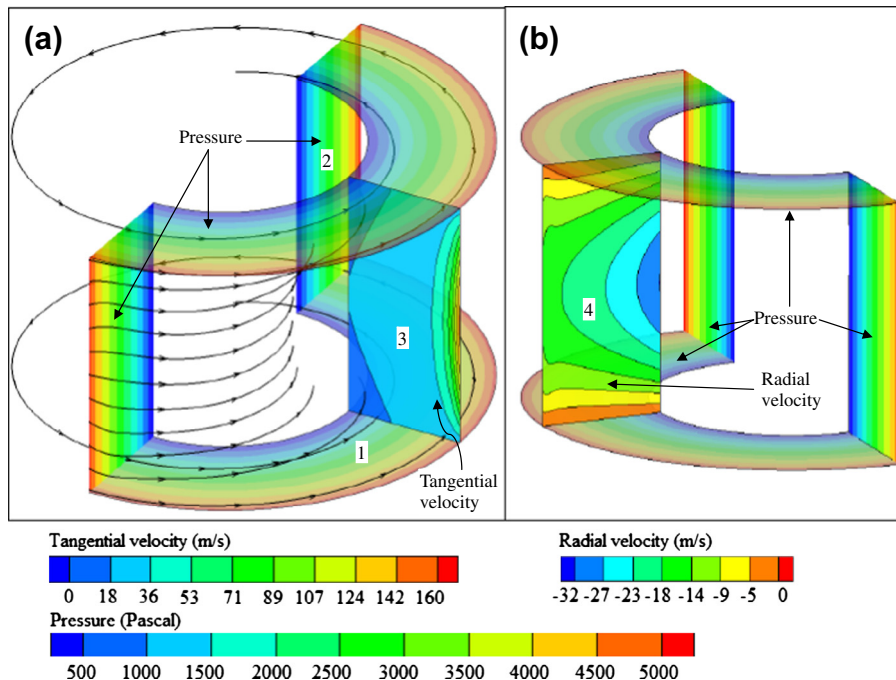


Fig. 10. (Colour online) Absolute pathlines, pressure and velocity field in the computational domain obtained from CFD analysis. Plane 1: Radial pressure distribution from inlet to exit (a), Plane 2: Pressure distribution in  $z$ -direction between the two discs (a), Plane 3: Tangential velocity from inlet to exit between the two discs (a), Plane 4: Radial velocity from inlet to exit between the two discs (b).

4. Tangential velocity at the disc surfaces equals the disc velocity (no slip condition) and it gradually increases to a maximum value at the middle of the disc spacing (see plane 3 in Fig. 10a).
5. Radial velocity progressively increases in the  $r$ -direction towards the exit (see plane 4 in Fig. 10b).
6. Radial velocity is zero on the surface of both discs and gradually increases to a maximum value at the middle of the disc spacing (see plane 4 in Fig. 10b).
7. Absolute pathlines starting from various  $z$ -locations move towards the exit in a nearly spiral path. Close to the disc wall, the length of the pathlines is larger due to lower values of radial velocity.

The above observations highlighted from the CFD simulations justify some of the assumptions used for the mathematical theory. It is to be realised that both CFD solutions and analytical solutions are subject to various assumptions; only the additional assumptions made in the analytical formulation can be verified by comparing the analytical results with CFD solutions. Thus, for example, the assumptions of laminar flow or no slip boundary condition – which are common to both CFD and analytical formulations – cannot be verified merely by comparing the two results. On the other hand, axisymmetric condition (i.e. no variation of flow variables in the  $\theta$ -direction) is applied for the mathematical theory, whereas the flow variables are allowed to vary in the  $\theta$ -direction in the CFD simulation. Therefore, the CFD solution given in Fig. 10 demonstrates the appropriateness of the axisymmetry assumption in the mathematical theory. Similarly, the pressure is allowed to vary in the  $z$ -direction in the CFD simulation. Hence, the near-constancy of pressure in the  $z$ -direction shown in the numerical simulations of Fig. 10 demonstrates the validity of Eq. (4) used in the mathematical theory.  $U_z$  is neglected in the mathematical theory: the fact that  $U_z$  is negligible as compared to  $U_r$  and  $U_\theta$  can be verified from the orientations of the pathlines (Fig. 10) which are almost parallel to each other. Detailed quantitative analysis of the velocity profiles produced by the CFD simulation also justifies the assumption of parabolic profiles, embodied in Eqs. (10) and (11), in the mathematical theory.

In this paper, the CFD simulations are presented only for an inter-disc spacing of 100  $\mu\text{m}$ . Further work is currently in progress; preliminary results suggest that the mathematical theory would be able to predict the torque up to larger disc spacings, though deviations may develop in the three-dimensional flow field.

## 7. Conclusion

The three-dimensional flow field and the flow pathlines within a Tesla disc turbine have been investigated analytically and computationally. For small values of inter-disc spacing, the predictions of the mathematical theory agree well with the results of detailed three-dimensional CFD simulations. It can be concluded from the results of CFD simulation that pressure does not vary in the  $z$ -direction (thus justifying Eq. (4)), whereas it decreases in the  $r$ -direction continuously from inlet to outlet. The radial velocity progressively increases in the  $r$ -direction towards the exit. At a particular radial location, both radial velocity and relative tangential velocity are functions of  $z$ -coordinate, are zero on the surface of both discs and gradually increase to a maximum value at the middle of the disc spacing. Absolute pathlines starting from various  $z$ -locations between two rotating discs move towards the exit in a nearly spiral path. Close to the disc wall, the length of these pathlines is larger due to lower values of radial velocity. The above observations highlighted from the CFD simulations justify some of the assumptions made previously for developing the mathematical theory and verifies some of the predictions of the theory.

The details of trajectories of fluid particles as a function of various flow parameters and turbine geometrical parameters have been thoroughly studied. The conclusions from such studies – for example, how the length, shape and orientation of pathlines depend on the values of tangential speed ratio  $\gamma$ , nozzle angle  $\alpha_n$ , radial pressure drop  $\Delta p_{ic}$  or radius of exit  $r_1$  – are given in the respective sections. One striking finding of the present study is that the length, shape and orientation of the relative pathlines change by modest amounts even when  $\gamma$  is changed by a large factor when  $\gamma > 1$ , and, these characteristics of relative pathlines become almost insensitive to changes in  $\gamma$  when  $\gamma$  is very large (say, for  $\gamma > 10$ ). The changes in the length, shape and orientation of the relative pathlines with a change in the value of  $\gamma$  are, however, significant for  $\gamma < 1$ .

Fluid particle trajectories in both absolute and relative frames of reference have been considered. It is established here that, although it may seem that the absolute and relative pathlines are merely two different ways of visualising the same flow, several subtle flow physics, such as flow reversal and the role of Coriolis force in establishing complex flow features, can only be appreciated when the relative pathlines are analysed.

## References

- [1] Ferrel W. An essay on the winds and the currents of the Oceans'. Nashville J Med Surgery 1856;11:287–301.
- [2] Wang HP, Olson SJ, Goldstein RJ, Eckert ERG. Flow visualization in a linear turbine cascade of high performance turbine blades. J Turbomach 1997;119(1):1–8.
- [3] Yang WJ. Handbook of flow visualization, 2nd ed.. Taylor & Francis Group; 2001.
- [4] Ferreira C, van Kuik G, van Bussel G. Wind tunnel hotwire measurements, flow visualization and thrust measurement of a VAWT in skew. In: 44th AIAA aerospace sciences meeting and exhibit, Reno, United States; 2006. p. 1–21.
- [5] Lee SW, Moon HS, Lee SE. Tip gap height effects on flow structure and heat/mass transfer over plane tip of a high-turning turbine rotor blade. Int J Heat Fluid Flow 2009;30(2):198–210.
- [6] Tesla N. Turbine. US Pat. 1 061 206; 1913.
- [7] Sengupta S, Guha A. A theory of Tesla disc turbines. Proc IMechE Part A: J Power Energy 2012;226(5):650–63.
- [8] Guha A, Smiley B. Experiment and analysis for an improved design of the inlet and nozzle in Tesla disc turbines. Proc IMechE Part A: J Power Energy 2010;224:261–77.
- [9] Guha A. A unified theory for the interpretation of total pressure and temperature in two-phase flows at subsonic and supersonic speeds. Proc R Soc 1998;454:671–95. <http://dx.doi.org/10.1098/rspa.1998.0180>.
- [10] Guha A. Computation, analysis and theory of two-phase flows. Aeronaut J 1998;102(1012):71–82.
- [11] von Kármán T. Über laminare und turbulente Reibung. Z Angew Math Mech 1921;1:233–52.
- [12] Batchelor GK. Note on a class of solutions of the Navier–Stokes equations representing steady rotationally-symmetric flow. Quart J Mech Appl Math 1951;4:29–41.
- [13] Stewartson K. On the flow between two rotating coaxial disks. Proc Camb Philos Soc 1953;49:333–41.
- [14] Dijkstra D, Van Heijst GJF. The flow between two finite rotating disks enclosed by a cylinder. J Fluid Mech 1983;128:123–54.
- [15] Zhou M, Garner CP, Reeves M. Numerical modelling and particle image velocimetry measurement of the laminar flow field induced by an enclosed rotating disc. Int J Numer Methods Fluids 1996;22:283–96.
- [16] Sandilya P, Biswas G, Rao DP, Sharma A. Numerical simulation of the gas flow and mass transfer between two coaxially rotating disks. Numer Heat Transfer 2001;39(A):285–305.
- [17] Andersson HI, Rousselet M. Slip flow over a lubricated rotating disk. Int J Heat Mass Transfer 2006;27:329–35.
- [18] Arora RC, Stokes VK. On the heat transfer between two rotating disks. Int J Heat Mass Transfer 1995;15:2119–32.
- [19] Jiji LM, Ganatos P. Microscale flow and heat transfer between rotating disks. Int J Heat Fluid Flow 2010;31:702–10.
- [20] Guha A, Sengupta S. The fluid dynamics of the rotating flow in a Tesla disc turbine. Eur J Mech – B/Fluids 2013;37:112–23.
- [21] Guha A. Optimisation of aero gas turbine engines. Aeronaut. J 2001;105(1049):345–58.
- [22] Guha A. Performance and optimization of gas turbines with real gas effects. Proc IMechE Part A: J Power Energy 2001;215(4):507–12.
- [23] Rice W. Tesla turbomachinery. In: Logan E, editor. Handbook of turbomachinery. New York: Marcel Dekker; 2003. p. 861–74.
- [24] Lemma E, Deam RT, Toncich D, Collins R. Characterisation of a small viscous flow turbine. Exp Thermal Fluid Sci 2008;33:96–105.

- [25] Hoya GP, Guha A. The design of a test rig and study of the performance and efficiency of a Tesla disc turbine. *Proc IMechE Part A: J Power Energy* 2009;223(A4):451–65.
- [26] Rice W. An analytical and experimental investigation of multiple-disk turbines. *ASME Trans J Eng Gas Turbines Power* 1965;87(1):29–36.
- [27] Deam RT, Lemma E, Mace B, Collins R. On scaling down turbines to millimetre size. *ASME Trans J Eng Gas Turbines Power* 2008;130(5):052301-1–1-9.
- [28] Carey VP. Assessment of Tesla turbine performance for small scale solar Rankine combined heat and power systems. *ASME Trans J Eng Gas Turbines Power* 2010;132(12) [Art. No. 122301].
- [29] Romanin VD, Carey VP. An integral perturbation model of flow and momentum transport in rotating microchannel with smooth or microstructured wall surfaces. *Phys Fluids* 2011;23(8) [Art. No. 082003].